Experimental study of axial flow in a vortex ring

Takashi Naitoh, Naohiko Fukuda, Toshiyuki Gotoh, Hideo Yamada, and Kei Nakajima
Department of Systems Engineering, Nagoya Institute of Technology, Gokiso-cho, Showa-ku, Nagoya 466-8555, Japan

(Received 12 April 2000; accepted 10 September 2001)

For a vortex ring at Re=1600, it was found that two types of azimuthal flow (axial flow) exist inside the vortex tube. The axial flow appears when the amplitude of a wavy deformation of the vortex ring becomes appreciable. The axial flow starts to grow before the wave-breaking and its speed increases gradually. In order to investigate the relation between the deformation of the vortex core and the axial flow, the flow field was examined experimentally using smoke visualization and the smoke wire technique simultaneously. Axial flow velocities are estimated from flow visualization images.
 [DOI: 10.1063/1.1420745]

I. INTRODUCTION

A vortex ring is formed by ejecting a blob of fluid from a circular orifice or nozzle in a short time. If the ejection velocity is moderate, the vortex ring translates smoothly in the early stage of developments. After it moves downstream about $5D$ (D: diameter of the vortex ring), perturbations are amplified due to the Widnall instability, and the vortex ring becomes wavy (Lim and Nickels[1]). The wave amplitude increases with time, and when it exceeds a threshold value the whole vortex ring quickly becomes turbulent. This transition process has been studied theoretically by Widnall, Bliss, and Tsar,[2] experimentally by Maxworthy,[3] Naitoh, Imai, Gotoh, and Yamada,[4] and Mochizuki, Kiya, Wakatsuki, Tanaka, and Suzuki,[5] and numerically by Shariff, Verzicco, and Orlandi.[6] The motion of the vortex with simple geometry is not only interesting in a fluid mechanical context but also has important engineering applications such as jets and wakes behind a circular body. It is now widely recognized that control of the transition to turbulence of a vortex ring is very important for engineering applications.

A flow inside the vortex ring core has been observed, when the amplitude of the wave on the vortex ring becomes significant. Moore and Saffman,[7] and Maxworthy[3] called it an axial flow. They inferred that this axial flow serves to reduce the amplification rate of waves and to change the wave number of the largest amplification rate. However, many aspects of the nature of the axial flow are still not well understood.

To our knowledge, experimental studies of the axial flow on a circular vortex ring are very few. Maxworthy[3] carried out experiments systematically over a wide range of Re_M, defined by $\mathrm{Re}_M = U_M \cdot D_M / \nu$ (U_M: average ejection velocity from the nozzle; D_M: nozzle diameter; ν: kinematic viscosity). (Also see Weigand.[8]) In the case of high Re_M (4.6×10^4 and 7.4×10^4), he found an axial flow along the turbulent ring which takes the form of a propagating wave like a solitary wave. He explained the cause of the axial flow as follows: ''At the high Re_M, the breaking of waves on vortex core due to Widnall instability does not take place uniformly and the azimuthal pressure gradients associated with this nonuniformity create a local azimuthal flow.'' Moreover, he said, ''At low Re_M, the wave breaking process is much more uniform and the axial flow, if one exists, is very weak.''

However, the physics of the axial flow inside the vortex ring is not well known. Further study of the axial flow is certainly needed. In the present study, we examine vortex rings at low Reynolds numbers in the transition process from a laminar to a turbulent state, focusing on the shape of the vortex core and the existence of the axial flow. Two types of axial flows that start to grow at the instant when the amplitude of wavy deformation of the vortex ring becomes appreciably large. Their velocities were estimated using flow visualization.

II. EXPERIMENTAL APPARATUS AND METHOD

Figure 1 is a schematic of the experimental apparatus. A loudspeaker is set on a plenum chamber box measuring 510 mm high, 510 mm wide, and 100 mm long. On the opposite side, the box has an orifice with a diameter of 50 mm. By applying a stepped voltage to the loudspeaker, air is almost instantaneously ejected from the orifice. Then a shear layer separates from the edge of the orifice, rolls up, and forms a vortex ring, which propagates in the test section [1150(L)*510(W)*510(H) mm] made of transparent acrylic resin plates. The vortex ring is illuminated by two 650 W halogen lumps on one side of the test section and the image is recorded by a digital video camera (Canon MV1, progressive mode, shutter speed: 1/250 s) mounted facing the ring. In order to focus on the propagating vortex ring, the camcorder is moved at the same velocity as the vortex ring.

The shape of the vortex ring is visualized by using the smoke from sticks of incense burned in the plenum chamber, and the axial flow can be observed by the movement of smoke injected into the vortex core locally using the smoke wire technique. The density of the incense smoke is set rather thin to bring out the contrast between the smoke of both methods. A Nichrome wire with a diameter of 50 μm is used for the smoke wire technique and is set just behind the orifice, as shown in Fig. 2.

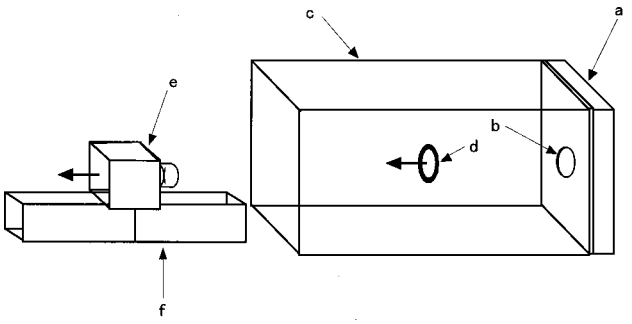

FIG. 1. Schematic of experimental apparatus; (a) plenum chamber with loudspeaker; (b) orifice; (c) test section; (d) vortex ring; (e) digital video camera; (f) camera transporter.

Since even a small deformation of the vortex ring affects the axial flow, the experiments were carefully arranged to avoid disturbances. A circular orifice and a wavy orifice were used. The latter was developed by Mochizuki, Kiya, Wakatsuki, Tanaka, and Suzuki[5] to produce a vortex ring with a stable wave number and phase. The edge of the wavy orifice is formed sinusoidally, and the number and amplitude of its wave are 9 and 2.5 mm, respectively. When the circular orifice was used, the number of the wave on the wavy orifice was determined by observing the most enhanced number of the wave on the vortex ring. The vortex ring generated from a wavy orifice is less sensitive to disturbances than that from a circular orifice, and the degree of periodicity of the azimuthal wave shape and the reproducibility are improved.

The Reynolds number is defined as $\mathrm{Re}=UD/\nu$, where U and D are the initial traveling velocity and the diameter of the vortex ring, respectively, and ν is the kinematic viscosity of air. Under the present experimental conditions, $U=49\,\mathrm{cm/s}$, and $D=4.9\,\mathrm{cm}$, and thus $\mathrm{Re}=1600$. The time at which a stepped voltage is applied to the loudspeaker is chosen as the origin of the reference time nondimensionalized by U and D.

III. RESULTS

A. Overview of axial flow

The azimuthal movement of tracer particles visualized by the smoke wire technique is complicated and its reproducibility is variable. The shape of the vortex core is slightly different for each run due to small external disturbances, and a slight deformation of the shape readily affects the smoke movement. Therefore, in spite of apparently identical experimental conditions, different modes of axial flow often occur, and in some cases no axial flow is observed.

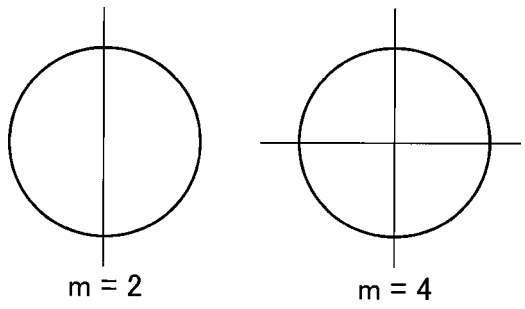

FIG. 2. Smoke wire arrangement on an orifice plane.

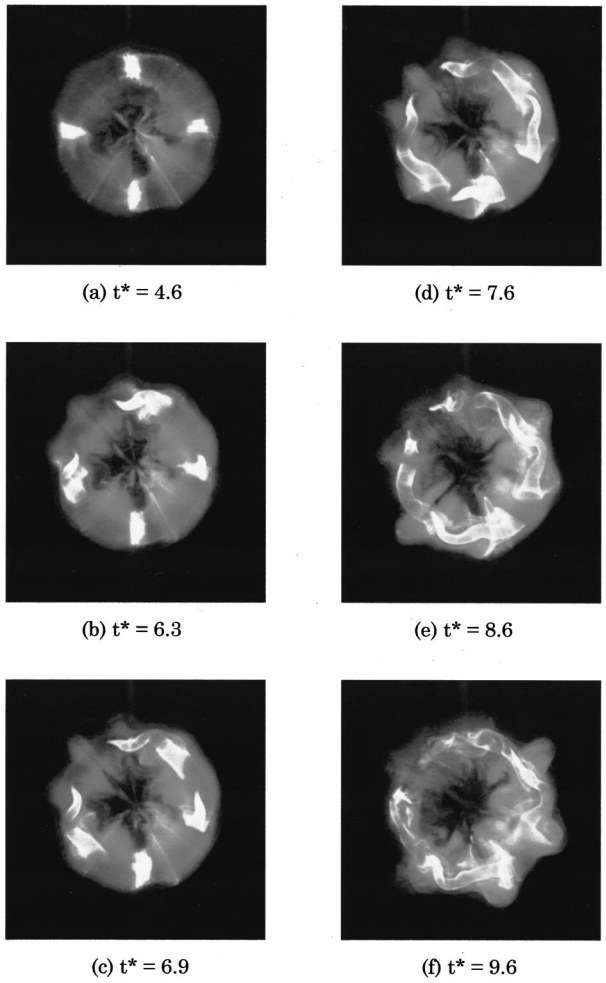

FIG. 3. Tops of the cone move toward upper left, where the amplitude of the wave is most increased.

In the following, we describe two typical axial flow patterns referred to as (i) the $m=1$ mode, and (ii) the $m=0$ mode, where m denotes the azimuthal wave number.

1. m=1 mode

Figure 3 shows frontal views of the vortex ring at $\mathrm{Re}=1600$, which are taken from the downstream direction. Two smoke wires are set on the circular orifice, as shown in Fig. 2. Paraffin liquid was applied to four short sections of the wires near the edge of the orifice and an electric current was applied for 5 ms, when a step voltage was applied to the loudspeaker. The smoke of oil mist was injected to four parts of the vortex core, as shown in Fig. 3(a). Such smoke is contained in part of the core when the shear layer separates from the edge of the orifice and rolls up, so that the streaklines made by this smoke form a spiral, as schematically shown in Fig. 4(a). It can be seen from Fig. 3(a) that the smoke generated from wires does not spread azimuthally as long as the vortex ring shape remains circular.

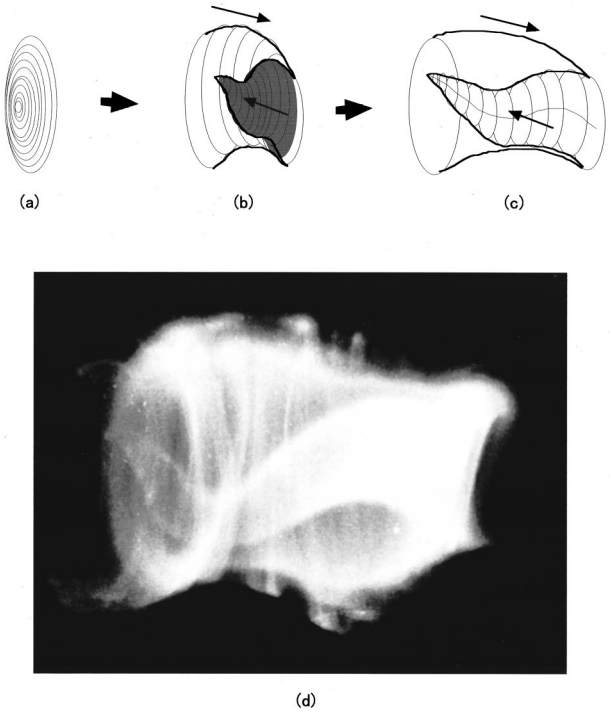

FIG. 4. Smoke pattern drifting along the vortex tube.

After the stage of development shown in Fig. 3(b), an axial flow appears as the amplitude of the azimuthal wave on the vortex increases. The existence of the axial flow can be determined by whether or not the smoke generated from the wire is stretched and becomes conical in shape, as schematically shown in Figs. 4(b) and 4(c). Hereafter we call this shape a cone. In Figs. 4(b) and 4(c), undulating cones are drawn along the vortex tube. The undulated axis of the cone and the axis of the envelope of the vortex tube have a phase difference of π as observed in Fig. 4(d), which is a view taken from the top of the vortex ring using a 35 mm still camera. The formation of cones means that the axial velocity varies with the distance from the vortex core center, as depicted in Fig. 5. In this figure, the change in flow direction in the central portion and surrounding area of the vortex core is indicated; this velocity profile may result simply from mass conservation within the vortex core.

As for the envelope shape of the vortex ring, the azimuthal wave is most amplified on the upper left part at the stage shown in Fig. 3(c). This wave, which is inferred to grow at 45 degrees in the direction of the vortex ring propagation (Maxworthy[3] and Shariff, Verzicco, and Orlandi[6]), has neither propagated azimuthally nor rotated until this stage. After that, the amplitude of the wave changes remarkably in

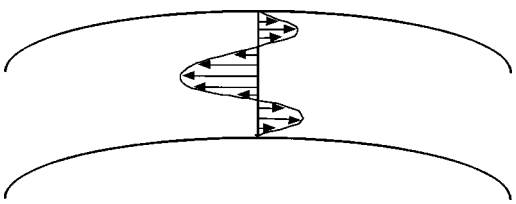

FIG. 5. Velocity profile of axial flow in a vortex tube.

TABLE I. The number of appearances of axial flow under each experimental condition.

	$m=1$ mode	$m=0$ mode	No regularities
Circular orifice with two smoke wires	45/49	0/49	5/49
Wavy orifice with one smoke wire	14/33	11/33	8/33

time as observed in the upper left part of Figs. 3(c) and 3(d). Thus, we infer that this part of the vortex ring begins to rotate locally and breaks at the stage seen in Fig. 3(e). This wave-breaking process propagates toward the lower right part through both sides of the vortex ring. At the stage of Fig. 3(e), the wave amplitudes of the upper right and lower left parts become larger, which is very similar to the state of Fig. 3(c), and then the wave collapses as shown in Fig. 3(f). Finally, the whole vortex ring becomes turbulent.

Now we consider the growth of the cones. In Fig. 3(c), the upper and left cones become 2–3 cm long and the right one begins to grow. Then, when the wave starts to rotate as shown in Fig. 3(d), the lower cone also begins to grow, and the upper and right cones grow to about 3.8 cm long, which corresponds to one-fourth of the ring circumference. Moreover, the top of the right cone enters into the bottom of the upper cone. The tops of the upper and right cones move counterclockwise, whereas the lower and left ones move clockwise. In other words, the tops of all the cones move toward the upper left, where the amplitude of the wave increases remarkably in the central region of the vortex core, and the bottoms of the cones move toward the lower right in the surrounding region of the vortex core. At the wave-breaking stage, shown in Fig. 3(e), the tops and bottoms of the cones have arrived at the upper left and lower right, respectively, and the growth of the cones ceases.

Supposing that the Widnall instability with $m=9$ dominates the phenomena, implies that the vortex ring is divided into nine cells along the ring, and that any perturbations on the velocity and/or vorticity have nodes at the cell boundaries, that is, changes occur completely within each cell. However, as seen in Fig. 3(e), the top of the right cone enters through the bottom of the upper cone, and at that instance the angle Θ of the upper cone is about 110° and the angles of the other cones are also greater than 80°, which is larger than 40° ($=360/9$) for one cell. The observation from Figs. 3(a)–3(f) clearly shows that the axial flow is generated, grows, and attains to a certain length scale longer than the wavelength predicted by the Widnall instability. The amplitude of the wavy deformation is already so large that the linear stability analysis, justified only for infinitesimally small perturbations, cannot be applied. Therefore, it is reasonable to think that the axial velocity observed is generated by some nonlinear mechanism.

The case shown in Fig. 3 was selected from among 49 runs under the same experimental conditions because this case shows the typical growth of cones, and its contrast be-

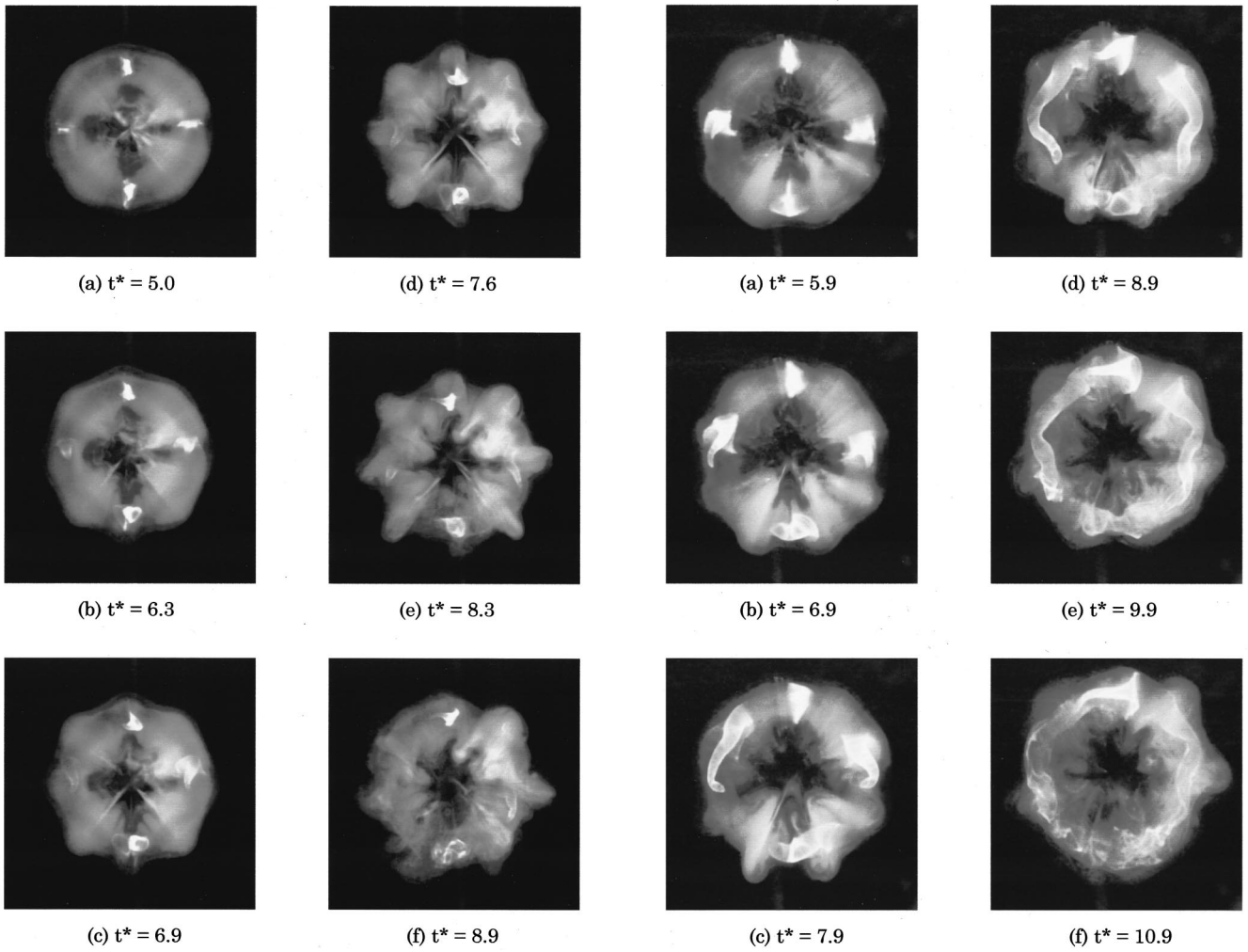

FIG. 6. The cones did not grow as well as expected under the same condition as in Fig. 3.

FIG. 7. The tops of the cone move toward the lower left, where the amplitude of the wave is most increased.

tween two kinds of smoke is strongest. In the other cases, the number of times each flow pattern appears is indicated in Table I. We can distinguish the appearance of $m=1$ mode cones in about 90% of 49 runs, but not in the remainder because of the irregularity of the tracer particle movement.

Figure 6 shows another run under the nominally same conditions as those of Fig. 3, and the axial flow does not appear. From the envelope shape of the vortex ring in the figure, we cannot specify the place where the amplitude of the wave is increasing locally. In other words, in the case where the amplitude of the wave increases uniformly, the axial flow tends not to appear.

From these observations, we inferred the generation mechanism of this type of axial flow as follows. As the amplitude of azimuthal wave increases, the vortex tube is locally stretched. According to Helmholtz's vortex theorem, the cross section of the stretched vortex tube shrinks and the vorticity increases, so that the pressure in the core locally decreases. In Fig. 3, the amplification rate of the azimuthal wave is higher in the upper left part than in the other parts. Consequently, a pressure gradient is induced in the vortex core in the azimuthal direction since the core cross section changes along the core, and the top of the cone moves toward the upper left, where the cross section is smallest.

Additional experiments were conducted in order to verify our speculations on the generation mechanism for the axial flow. In order to increase the amplitude of the wave at different places, we tried to intentionally disturb a vortex ring. We set three circular cylinders (diameter 0.5 mm) on the orifice plane, which protruded 2 mm inward normal to the edge at the upper right part at regular intervals. Other experimental conditions were the same as those in Fig. 3. We found that the wave amplitude starts to quickly increase at the lower left position [see in Fig. 7(b)], and the tops of the cones move toward the lower left, as seen in Figs. 7(c)–7(e). These results support our earlier conjecture.

2. m=0 mode

Figure 8 shows the frontal views of the vortex ring at Re=1600, which is generated using the wavy orifice and visualized with one vertical smoke wire. It was found that the time necessary for the azimuthal wave to develop was shorter than that of a vortex ring generated from the circular orifice. The azimuthal wave appears earlier, the effects of disturbances become relatively smaller, and the number and

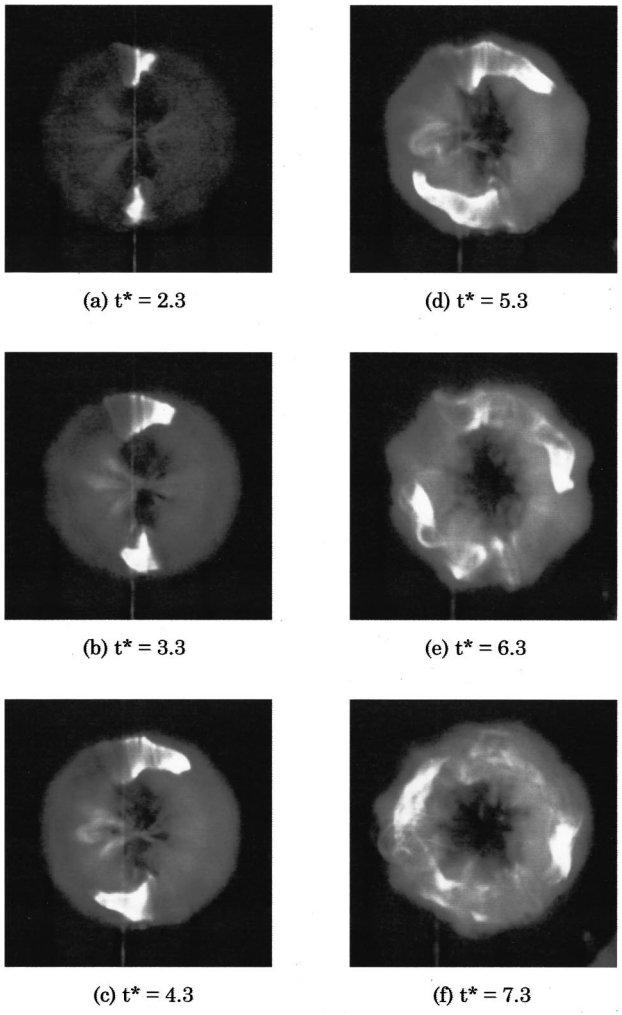

FIG. 8. The tops of the cone turn around clockwise when the waviness is amplified uniformly.

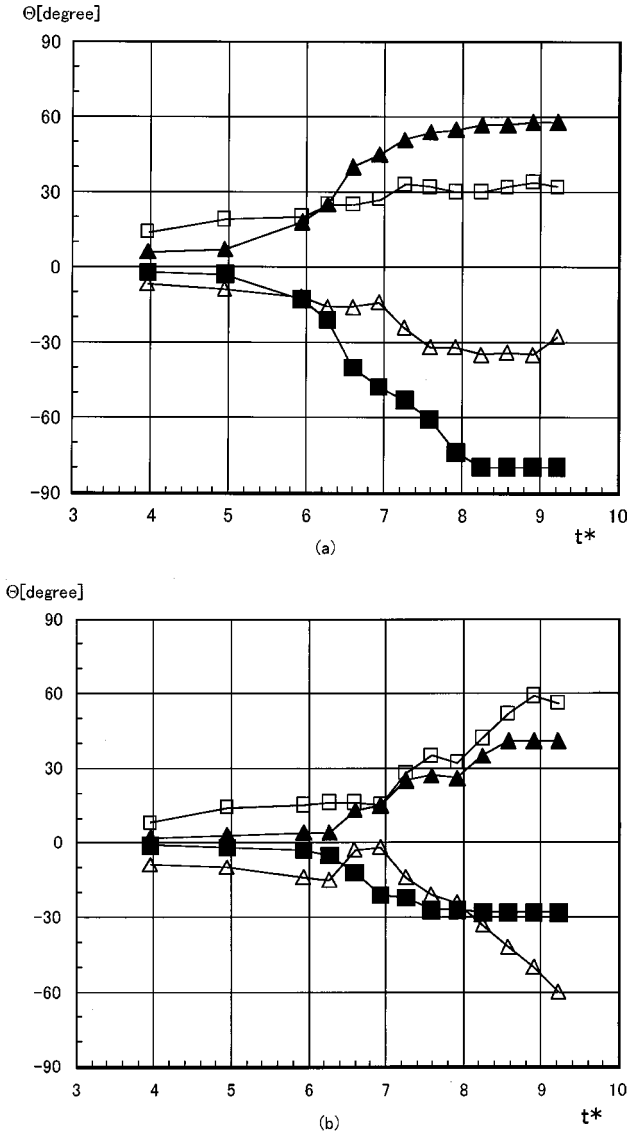

FIG. 9. The relative positions of cones in the case of Fig. 3; (a) the upper and left cones; □: the top of the upper cone; ■: the bottom of the upper cone; △: the top of the left cone; ▲: the bottom of the left cone. (b) The lower and right cones; □: the top of the right cone; ■: the bottom of the right cone; △: the top of the lower cone; ▲: the bottom of the lower cone.

phase of waves are fixed spatially, so that the reproducibility of wave shape and the degree of periodicity of azimuthal shape are improved. The growth of the cones always starts with development of the azimuthal wave. Then, the cones of the vortex ring generated from the wavy orifice appear earlier than those from the normal circular orifice. For example, the cones in Fig. 8(b) start to grow at $t^*=3.3$, while at $t^*=6.3$ in Fig. 3(b), in the case of the circular orifice. As for the breaking of the azimuthal wave, the breaking time in Fig. 8 decreases by a factor of 1.4 compared with the flow shown in Fig. 3.

Smoke injected into the upper and lower part of the vortex core, respectively, forms the cones. [Smoke of incense sticks, which visualizes the envelope form of a whole vortex ring, is not visible in Fig. 8(a), because the light had to be dimmed in front of the orifice.] The cone tops grow clockwise as time elapses. The azimuthal wave on the vortex ring generated from the wavy orifice grow more uniformly than that from a circular orifice. (We rarely observe a case in which the amplitude of the wave increases locally as in Fig. 3.) When the wave growth is uniform azimuthally, the cones are apt to grow in the same direction, clockwise or counterclockwise.

Out of the 33 runs, 11 times the $m=0$ mode and 14 times the $m=1$ mode were counted (Table I). For the other eight runs, well-developed cones were not observed due to halting the growth of cones or low image contrast.

B. Axial flow velocity estimates

In order to estimate the axial flow velocity and to understand the process of the cone evolution, the locations of the tops and bottoms of the cones were measured and shown in Fig. 9; these data are obtained from images of Fig. 3. The horizontal axis is the nondimensional time and the vertical one is the angle Θ subtended to the center of the vortex ring, where the arclength is measured from the location of the smoke wire to the top or bottom of each cone. It is evident

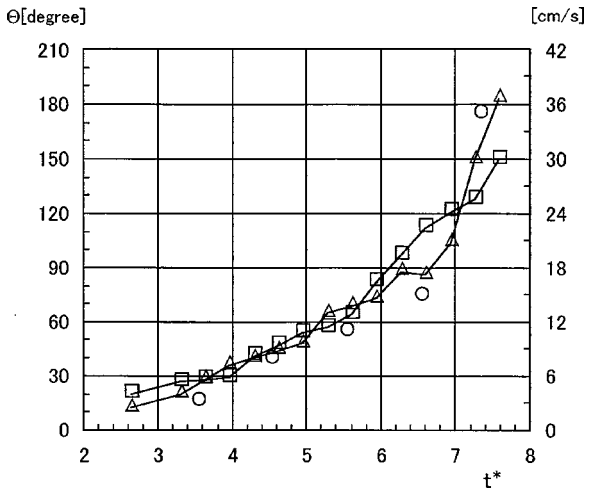

FIG. 10. The relative positions of cones in the case of Fig. 6, □: the top of the upper cone; △: the top of the lower cone; ○: averaged axial velocity.

from Fig. 3 that the flow field is approximately symmetric with the plane passing from upper left to lower right at the angle of 45° to the vertical line. The data of the upper and left cones are plotted in Fig. 9(a), and those of other cones are plotted in Fig. 9(b). Both Figs. 9(a) and 9(b) are roughly symmetrical with the line of the $\Theta=0$ degree. The cones abruptly grow at about $t^*=6.0$ in Fig. 9(a) and at about $t^*=7.0$ in Fig. 9(b). After the breakdown of the azimuthal wave at $t^*=7.6$ (as determined from images of visualization), the smoke forming the cones continues to move azimuthally inside the vortex core. The upper and left cones start to grow earlier than the right and lower cones and cease to grow at $t^*=8.0$, while the latter keep growing until $t^*=9.0$.

We observe as plane images the evolution of the cones along a vortex tube that is distorted complicatedly in three-dimensional space. Moreover, since the camcorder records 30 frames per second, and the shape of the cone sometimes changes quickly, the time resolution of the successive images is not enough for the present flow field. For these reasons, it is difficult to evaluate the axial flow velocity accurately, so that we can only estimate the representative axial velocity approximately from the slopes of the curves in Fig. 9. The average axial velocity is thus found to be 10–13 cm/s in the sections where gradients are steep; for example, the bottom of the upper cone ($t^*=6.0-8.0$), the top of the right cone ($t^*=7.0-9.0$), the top of the lower cone ($t^*=6.0-8.0$), and so on. This average velocity corresponds to between 1/5 and 1/4 of the vortex ring propagation velocity. The maximum axial velocity, which is estimated from just two successive frames, is approximately one-half of the vortex ring propagation velocity.

Regarding the case of $m=0$ mode (Fig. 8), the axial velocity may be obtained in the same way as in Fig. 3, and the result is shown in Fig. 10. The growth of the cones shows a similar tendency for both the upper and lower cones, and the axial velocities increase as time elapses. The average velocity for each unit interval of time is also indicated in Fig. 10. The velocity increases as the amplitude of the wave on the vortex core increases, so that it reaches about one-fourth of the ring propagation velocity when the wave breaks at $t^*=6.2$. After that, the velocity further increases, and the ultimate velocity that we can estimate is approximately half the ring propagation velocity.

C. Effects of smoke wire

In the present experiment, one or two pieces of Nichrome wire (diameter 50 μm) were located on the orifice plane, as shown in Fig. 2. It seems reasonable to expect that one piece of wire would excite a disturbance with periodicity $m=2$ and two pieces of wire with periodicity $m=4$ at the unstable stage of a vortex ring under the present conditions.

However, it was shown by Naitoh, Sun, and Yamada[9] that the wire does not change the flow field substantially, and that there is little influence of the thin wires on the visualization results of the vortex ring. The number of the azimuthal wave appearing in the final stage of the laminar state is 9, not a multiple of 2 or 4. This means that the periodicity by the Widnall instability is predominant over the one by wires.

IV. CONCLUSIONS

An azimuthal flow inside a vortex tube, which appears when the amplitude of a wavy deformation of the vortex ring becomes appreciable, was investigated using the smoke visualization method and the smoke wire technique simultaneously. Two types of axial flow were found to exist within the vortex ring at $\mathrm{Re}=1600$. Both flows start to increase before the start of the azimuthal wave breaking and the flow velocities increase gradually, while the axial flow that Maxworthy[3] observed appears after the wave breaking and takes the form of a propagating wave. In the case of an $m=1$ mode, the average axial velocity is 10–13 cm/s after the amplitude of wavy deformation becomes appreciable. As for the case of an $m=0$ mode, the axial velocity reaches about 12 cm/s, which corresponds to one-fourth of the ring propagation velocity when the wave breaks at $t^*=6.2$. After that, the velocity increases further.

Although the presence and development of the axial flow in the vortex ring was documented, a complete explanation about the birth and growth of the axial flow awaits further work. Certainly this needs more studies.

ACKNOWLEDGMENTS

We are very grateful to Professor Alexander J. Smits, Dr. James J. Allen, and Juan M. Jimenez for their useful comments and critical reading of the manuscript.

[1] S. I. Green, T. T. Lim, and T. B. Nickels, *Fluid Mechanics and its Applications* (Kluwer Academic, Dordrecht, 1995), pp. 110–129.
[2] S. E. Widnall, D. B. Bliss, and C.-Y. Tsai, "The instability of short waves on a vortex ring," J. Fluid Mech. **66**, 35 (1974).
[3] T. Maxworthy, "Some experimental studies of vortex rings," J. Fluid Mech. **81**, 465 (1977).
[4] T. Naitoh, S. Imai, T. Gotoh, and H. Yamada, "Circumferential instability of a vortex ring," Nagare **15**, 401 (1996) (in Japanese).
[5] O. Mochizuki, K. Kiya, K. Wakatsuki, Y. Tanaka, and N. Suzuki, "Simultaneous observations of vortical structures and velocity fluctuations in vortex rings during a transition process," *Proceedings of the 7th Asian Congress of Fluid Mechanics*, 1997, pp. 159–162.

[6]K. Shariff, R. Verzicco, and P. Orlandi, ''A numerical study of three-dimensional vortex ring instabilities: viscous corrections and early nonlinear stage,'' J. Fluid Mech. **279**, 351 (1994).
[7]D. W. Moore and P. G. Saffman, ''The instability of a straight vortex filament in a strain field,'' Proc. R. Soc. London, Ser. A **356**, 413 (1975).
[8]A. Weigand, ''The response of a vortex ring to a transient spatial cut,'' *Proceedings of the 7th International Symposium on Flow Visualization*, 1995, pp. 140–145.
[9]T. Naitoh, B. Sun, and H. Yamada, ''A vortex ring traveling across a thin circular cylinder,'' Fluid Dyn. Res. **15**, 43 (1995).